Quaternary International xxx (xxxx) xxx–xxx

Contents lists available at ScienceDirect

Quaternary International

journal homepage: www.elsevier.com/locate/quaint

A stalagmite $\delta^{18}O$ record from Jinfo Cave, southern China reveals early-mid holocene variations in the East Asian Summer Monsoon

Xunlin Yang[a,b,*], Ruikai Liu[a], Rui Zhang[a], Baoyan Wang[a], Riping Zhang[a], Yingran Yan[a]

[a] Key Laboratory of Eco-environments in Three Gorges Reservoir Region (Ministry of Education), School of Geographical Sciences, Southwest University, Chongqing, China
[b] Chongqing Key Laboratory of Karst Environment, Southwest University, Chongqing, China

ARTICLE INFO

Keywords:
Millennial-scale
Stalagmite
Summer monsoon
Holocene
Southern China

ABSTRACT

The stability of the East Asian Summer Monsoon (EASM) during the early Holocene and the timing of the Holocene optimum have been intensely debated. Both stalagmite and lake records from northern China imply that there was a millennium-scale monsoon weakening event during the early Holocene, but whether this phenomenon is common across the Asian monsoon region remains unclear due to a paucity of records from southern China. We present results from U–Th dating and 433 stable carbon and oxygen isotope datapoints in order to investigate variations in the EASM during the early-mid Holocene in southern China. The results show that stalagmite $\delta^{18}O$ values are relatively low in the period of 10.1–9.6 ka BP, indicating enhanced monsoon activity in the early Holocene. The stalagmite $\delta^{18}O$ values for the period of 9.1–8.1 ka BP are characterized by a "w" type oscillation, indicating that there was a period of monsoon recession. In contrast, the period of 8.0–6.0 ka BP is characterized by relatively low, implying a strong monsoon. The results of our study indicate there was a millennial-scale weakening of the monsoon during the early Holocene in southern China. This suggests that the early Holocene monsoon weakening events are widespread throughout the monsoon region of eastern China.

1. Introduction

The East Asian Summer Monsoon (EASM) plays a major role in global atmospheric thermodynamics. The associated precipitation has a direct impact on the socio-economic development of East Asia, the most densely populated region in the world (An et al., 2000; Wang et al., 2005). The Holocene is one of the key time intervals for understanding the relationship between changes in the EASM and human settlement and adaptations. The strength of the EASM in the Holocene has been argued to have profoundly impacted the trajectories of prehistoric societies and the replacement of historical dynasties (Dong et al., 2019; Xu et al., 2019; Zhang et al., 2008). Recently, the publication of a series of high-resolution palaeoclimatic records has enabled us to further understand the evolution of the Holocene EASM (An et al., 2000; Chen et al., 2015; Goldsmith et al., 2017; Lu et al., 2013; Maher and Thompson, 2012; Shi et al., 1994; Wang et al., 2005). However, the evolution of EASM during the Holocene still remains controversial (Cai et al., 2010; Cheng et al., 2015; Tan, 2009; Wang et al., 2005; Zhou et al., 2004).

Previous studies have been focused on the timing of the Holocene Optimum/EASM precipitation maximum, as well as fluctuations in the strength of the early Holocene EASM in different parts of China (An et al., 2000; Cheng et al., 2015; Shi et al., 1994; Zhou et al., 2004). Increasing research has shown that the early Holocene EASM may have been unstable (Dong et al., 2018; Yang et al., 2019; Zhang et al., 2018). For example, Yang et al. (2019) constructed a Holocene stalagmite $\delta^{18}O$ composite record and found that the early Holocene was relatively unstable with weaker monsoon events in the EASM region. Stable carbon and oxygen isotope records from stalagmites in northern China have revealed two weak monsoon events at 10-9.4 and 8.7-8.3 ka BP, which was presented as an asymmetric "w" shape in the curve and that interrupted the period of strong monsoon activity (Zhang et al., 2018). Dong et al. (2018) found that stalagmite $\delta^{18}O$ values increased during 9.5–8.1 ka BP from Lianhua Cave, and attributed this to a millennial-scale weakening of the monsoon in northern China during the early Holocene. Qinghai Lake records from northern China also show that there were at least two millennial-scale declines of EASM in the early Holocene (An et al., 2012). North China is the focus of paleoclimate research, because it is the cradle of Chinese civilization, but it is also facing serious ecological problems such as drought and desertification.

At present, records of changes in the EASM during the early-mid Holocene are primarily from northern China (Chen et al., 2015; Dong et al., 2018; Goldsmith et al., 2017; Zhang et al., 2018). However, there remains a significant question as to whether this event is widespread

* Corresponding author. Chongqing Key Laboratory of Karst Environment, School of Geographical Sciences, Southwest University, Chongqing, 400715, China.
E-mail address: xlyang@swu.edu.cn (X. Yang).

https://doi.org/10.1016/j.quaint.2020.01.002
Received 29 August 2019; Received in revised form 2 January 2020; Accepted 6 January 2020
1040-6182/

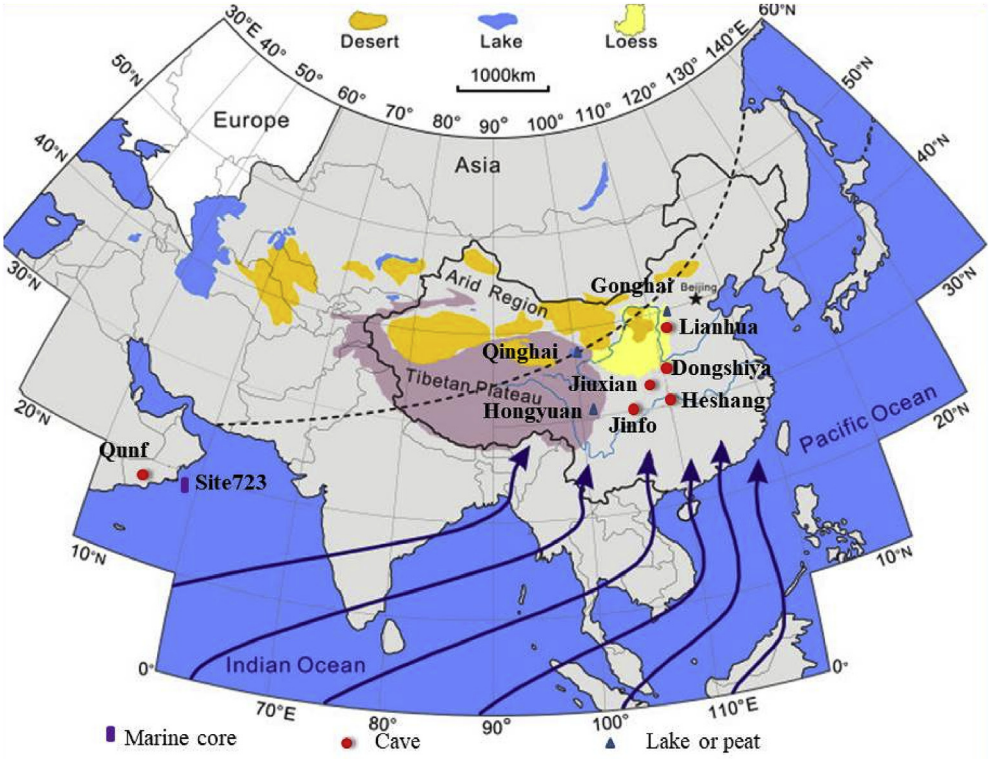

Fig. 1. Sites of Holocene summer monsoon records from the Asian region mentioned in the text (Modify according to Zhang et al., 2012). Lianhua Cave (Dong et al., 2015); Jiuxian Cave (Cai et al., 2010); Dongshiya and Laomu Cave (Zhang et al., 2015, 2018); Qunf Cave (Q5) (Fleitmann et a1., 2003); Heshang Cave (HS4) (Hu et al., 2008); Site723 from the Arabian Sea (Gupta et al., 2003); Gonghai Lake (Chen et al., 2015); Hongyuan (Hong et al., 2003); Qinghai Lake (An et al., 2012).

across the East Asian monsoon region, and whether shifts in precipitation, and their impacts on regional environments, vary between northern and southern China. Yet, detailed palaeoenvironmental and palaeoclimatic records for the Holocene are largely lacking from southern China. In addition, although stalagmite $\delta^{18}O$ records have been widely used for reconstructing precipitation fluctuations and EASM operation (Dong et al., 2018; Goldsmith et al., 2017; Zhang et al., 2018), it remains debated as to whether they provide a robust record of local precipitation amounts. Here we present a well-dated stalagmite (NO. J13) carbonate $\delta^{18}O$ and $\delta^{13}C$ record from Jinfo Cave to elucidate the spatio-temporal changes in EASM intensity in southwestern China since 10.5 ka BP to the late Holocene. In doing so, we fill a major regional gap in reconstructions of the operation of the EASM across China, and East Asia more broadly, during the Holocene, enabling more detailed understandings of leads and lags across terrestrial, marine, and atmospheric systems.

2. Site and regional climate, stalagmite samples and methods

2.1. Using $\delta^{18}O$ of stalagmites to interpret changes in the EASM

Speleothems possess unique advantages in the context of palaeoclimatic reconstruction as they can be precisely dated using U-series methodologies (Cheng et al., 2009, 2019a), meaning that they have been widely used on a global scale. Stable oxygen isotope measurements ($\delta^{18}O$) of speleothems have been used to determine changes in precipitation, however, interpretation is often complex as these values can be variously controlled by different factors including water vapour source, cave temperature during deposition, and local cave contexts (Chen and Li, 2018; Cheng et al., 2019a, 2019b; Maher, 2008; Perez-Mejías et al., 2018; Yang et al., 2014, 2019). For example, Cheng et al. (2019b) interpreted cave $\delta^{18}O$ from North America as reflecting changes in the annual balance of precipitation between summer and winter. Monitoring data from Ejulve Cave in Europe demonstrated that the $\delta^{18}O$ signal of modern calcite reflected the $\delta^{18}O$ value of drip-water, which was controlled mainly by the surface air temperature (Perez-Mejías et al., 2018). In many regions, the response of speleothem $\delta^{18}O$ to precipitation amounts is complicated due to the influence of various water vapour sources; therefore, there are still many controversies about the climatic significance of stalagmite in the EASM region (Cheng et al., 2019a; Maher, 2008; Tan, 2009; Wang et al., 2008; Yang et al., 2019; Yuan et al., 2004). For example, there are currently three interpretations of stalagmite $\delta^{18}O$ in the EASM region: 1) that stalagmite $\delta^{18}O$ represents the regional intensity of the EASM (Cheng et al., 2019a; Dong et al., 2015; Wang et al., 2008; Yang et al., 2019; Yuan et al., 2004), 2) that stalagmite $\delta^{18}O$ is an indicator of local precipitation amount (Zhang et al., 2008), and 3) that stalagmite $\delta^{18}O$ reflects shifts in water vapour sources (Maher, 2008; Tan, 2009).

Based on 16 stalagmite $\delta^{18}O$ records, Yang et al. (2019) concluded that $\delta^{18}O$ measurements track changes in EASM intensity across the East Asian monsoon domain, and are not solely indicators of precipitation at a particular cave site in each case. Nevertheless, Cheng et al. (2019a) have noted that the overall precipitation and seasonal precipitation reconstructions do vary across this highly diverse region. To interpret the Mt. Jinfo record, we utilize modern cave monitor (Chen and Li, 2018) that demonstrates that shifts in $\delta^{18}O$ precipitation in the region are closely related to atmospheric circulation patterns on inter-annual time scales. As a consequence, we argue that stalagmite $\delta^{18}O$ at Jinfo Cave is not just a local precipitation record but can also yield insights into the wider intensity of the EASM, with low $\delta^{18}O$ indicating a strong EASM and high $\delta^{18}O$ indicating a weaker EASM as has been noted elsewhere (Cheng et al., 2009, 2019a; Dong et al., 2015; Wang et al., 2008; Yuan et al., 2004).

The factors influencing speleothem $\delta^{13}C$ are complex and include changes in vegetation (including the dominance of C_3 or C_4 plants in the region and/or productivity), soil composition, atmosphere CO_2, hydrology (including the hydrodynamics of karst groundwater, water-rock interactions, calcite precipitation processes etc.) (Hendy, 1971; Li et al., 2012; Zanchetta et al., 2007). As a consequence, the application of $\delta^{13}C$ in palaeoclimatic and palaeoenvironmental reconstruction is not as widespread as $\delta^{18}O$. Based on the monitoring of $\delta^{13}C$ in cave systems, Li et al. (2012) argued that speleothem $\delta^{13}C$ could be used to

Table 1
Isotopic composition of uranium and thorium and ^{230}Th ages for Jinfo Cave speleothems as determined by MC-ICP-MS.

Sample Number	Depth	^{238}U		^{232}Th		δ^{234}U[a]		^{230}Th/^{238}U		^{230}Th Age (yr)		^{230}Th Age (yr)		$\delta^{234}U_{Initial}$[b]	
	(mm)	(ppb)		(ppt)		(measured)		(activity)		(uncorrected)		(corrected)		(corrected)	
JF13-1	0.15	5471	± 12	287	± 16	39	± 2	0.003	± 0.0002	273	± 23	272	± 23	39	± 2
JF13-2	0.5	4715	± 21	41	± 5	5416	± 3	0.003	± 0.0001	299	± 11	299	± 11	40	± 3
JF13-3	1.5	3964	± 6	172	± 11	43	± 2	0.005	± 0.0002	472	± 22	471	± 22	43	± 2
JF13-4	3.55	1930	± 4	376	± 16	24	± 3	0.018	± 0.0006	1980	± 67	1975	± 67	24	± 3
JF13-5	4.9	2390	± 4	319	± 8	32	± 2	0.02	± 0.0002	2178	± 26	2175	± 26	32	± 2
JF13-6	6.25	9037	± 17	99	± 14	34	± 2	0.023	± 0.0001	2440	± 15	2440	± 15	34	± 2
JF13-7	8.3	7286	± 19	154	± 6	45	± 2	0.041	± 0.0002	4417	± 23	4416	± 23	46	± 2
JF13-8	9.85	11211	± 31	600	± 16	62	± 2	0.045	± 0.0002	4675	± 26	4674	± 26	63	± 2
JF13-9	12.4	7360	± 17	293	± 9	39	± 2	0.05	± 0.0002	5395	± 26	5393	± 26	39	± 2
JF13-10	12.95	8164	± 17	202	± 12	41	± 2	0.051	± 0.0002	5491	± 29	5490	± 29	42	± 2
JF13-11	15.6	3198	± 7	364	± 13	25	± 2	0.061	± 0.0004	6703	± 46	6699	± 46	26	± 2
JF13-12	16.5	4756	± 9	704	± 15	14	± 2	0.067	± 0.0004	7539	± 33	7535	± 33	14	± 2
JF13-13	17.9	5605	± 15	144	± 6	17	± 3	0.076	± 0.0004	8498	± 48	8497	± 48	17	± 3
JF13-14	18.65	3977	± 7	356	± 14	35	± 2	0.083	± 0.0003	9097	± 43	9094	± 43	36	± 2
JF13-15	19.7	6459	± 13	90	± 4	40	± 2	0.094	± 0.0003	10349	± 39	10348	± 39	41	± 2
JF13-16	20.5	3572	± 10	274	± 7	20448	± 3	0.095	± 0.0005	10421	± 66	10419	± 66	45	± 3

[a] $\delta^{234}U = ([^{234}U/^{238}U]_{activity} - 1) \times 1000$.
[b] $\delta^{234}U_{initial}$ was calculated based on ^{230}Th age (T), i.e., $\delta^{234}U_{initial} = \delta^{234}U_{measured} \times e^{\lambda_{234} \times T}$. Corrected ^{230}Th ages assume the initial ^{230}Th/^{232}Th atomic ratio of $4.4 \pm 2.2 \times 10^{-6}$. Those are the values for a material at secular equilibrium, with the bulk earth ^{232}Th/^{238}U value of 3.8. The errors are arbitrarily assumed to be 50%.

track shifts in local vegetation in certain parts of the Chongqing karst. The δ^{13}C values of the Jinfo Cave stalagmite are unusually high for speleothems that is likely a product of the high δ^{13}C of the source rock and low construction from soil CO_2, something expected given that Mt. Jinfo is characterized by steep terrain, low soil coverage, and high altitude (Dreybrodt, 1982; Zanchetta et al., 2007). Since the rock δ^{13}C values are time-constant, periodic changes in soil CO_2 production are the factors most likely driving variation in δ^{13}C at Jinfo Cave.

2.2. Cave site and stalagmite sample

Stalagmite J13 was collected from Jinfo Cave (29°02′33″N, 107°10′45″E), Chongqing, which is located at the boundary between the Sichuan Basin and Yun-Gui Plateau, southwestern China (Fig. 1 and Fig. s1). This region is subject to typical EASM climate conditions with an average annual precipitation of 1384 mm and an average annual temperature of 8.2 °C in the upper part of the mountains (about 2000 m above sea level). Rainfall is concentrated in summer (April–October), accounting for 80.4% of the total annual precipitation (Chen and Li, 2018). Jinfo Cave has formed in carbonate rocks at an elevation of 2080 m in Mt. Jinfo with very low soil cover. The uppermost rock unit of Mt. Jinfo is Permian limestone, and a huge and complex underground cave system has developed within this unit. Stalagmite J13 is 210 mm long and was cut along the middle of its growth axis. It is composed of dark brown and yellow brown calcite, with an internal structure revealing a clear sub-millimeter scale layering. The part of stalagmite with darker color is dense, while the part with lighter color is loose. The cut surface of the stalagmite was polished with a polishing machine and revealed no obvious hiatus indicator of continuous deposition. Spectral analysis of the stalagmite J13 δ^{18}O record was carried out with the aid of the Past programme (Hammer et al., 2001).

2.3. U–Th dating

The stalagmite was first halved along growth axis and polished. 16 subsamples for ^{230}Th dating were obtained from the stalagmite. About 20–30 mg of powder was drilled near the central axis for each ^{230}Th dating subsample. The ^{230}Th age samples were measured using a Finnigan Neptune multiple-collector magnetic sector with inductively coupled plasma mass spectrometers following the analytical specifications detailed by Cheng et al. (2013) and Shen et al. (2012). The dating results of stalagmite J13 can be found in Table S1. The analytical uncertainties of the ages are equal to or less than 1%. All ages are in stratigraphic order within dating uncertainties. Because of the high ^{238}U content, the dating precision for stalagmite J13 is very high, and the age errors are less than 0.3%. Work was carried out at the isotope laboratory of the Department of Earth Sciences, University of Minnesota.

2.4. Stable isotope analyses

433 samples for stable isotope measurements were obtained from stalagmite J13. The subsamples were collected by dental drill or graver along the central growth axis of stalagmite J13, and the methods were described in Zhang et al. (2008). The δ^{18}O and δ^{13}C measurements were made with a Finnigan Delta V Plus fitted with a Carbonate Device (Kiel-II) in the Chongqing Key Laboratory of Karst Environment, Southwest University, China. The isotopic results were provided following the Vienna Pee Dee Belemnite standard with one-sigma external error $< \pm 0.1‰$ for δ^{18}O and $< \pm 0.06‰$ for δ^{13}C. Two carbonate reference standards (one is the international standard, i.e.NBS19, and the other is laboratory carbonate standard, i.e. SWU) were used for calibration to ensure that measurement precision (at 1σ) was higher than ± 0.1‰.

3. Results

3.1. Chronology

Uranium-thorium isotopic composition and ^{230}Th ages from stalagmite J13 are listed in Table 1. Age-depth plots are given in Fig. 2. In this paper, the stalagmite model was established using the Model Age software (Hercman and Pawlak, 2012). The stalagmite samples used in this study have high U contents, allowing us to obtain high-precision ^{230}Th dates. Most of the age errors are ± 30 years; with the minimum error being 11 years for all ages spanning the period 0.3–10.5 ka BP. The result shows that stalagmite J13 grew fast and continuously from 0.3 to 2.1 ka BP (0.03 mm/year), but slowly from 2.1 to 10.5ka BP (0.02 mm/year) (Table 1). The programme Model Age (Hercman and Pawlak, 2012) was utilized in order to establish a detailed chronology for exploring changes in the EASM reconstructed on the basis of stalagmite δ^{18}O (Fig. 2).

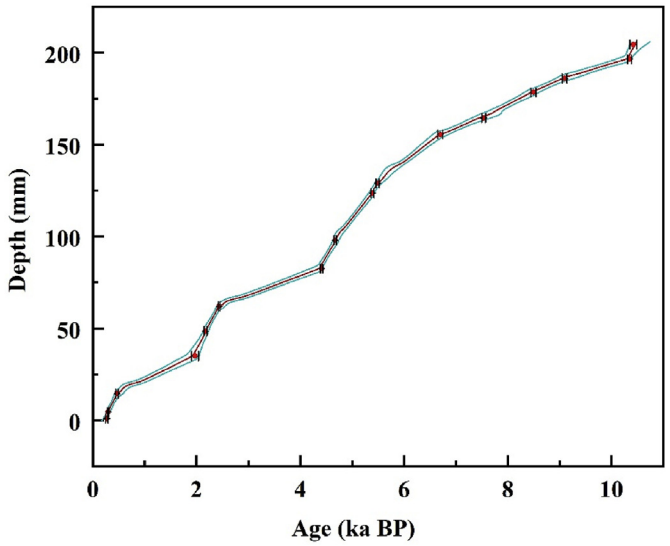

Fig. 2. Age-depth models for stalagmite J13 established with MOD-AGE software with 95% confidence interval (Hercman and Pawlak, 2012).

3.2. Stable isotope records

The $\delta^{18}O$ record is in phase with orbital precession-induced changes in solar radiation (Fig. 3). The $\delta^{18}O$ values vary from −6.7‰ to −9.6‰ during the Holocene, with the average value being −8.3‰. The $\delta^{18}O$ values began to decrease rapidly at 10.3 ka BP and reached the first peak near 10.0 ka BP and remained relatively low until 9.6 ka BP (average value −9.2‰). In comparison with stalagmite records from northern China (Dong et al., 2018; Zhang et al., 2018), the Jinfo Cave $\delta^{18}O$ record shows a "w" type oscillation during the period of 9.1–8.1 ka BP, noted by Zhang et al. (2018) in northern China. In particular, from 9.1 to 8.8 ka BP, the $\delta^{18}O$ value increased abruptly and reached the first trough of the "w" type oscillation at about 8.8 ka BP; then the curve began to rebound slowly. After 8.5 ka BP, the $\delta^{18}O$ profile increased again and reached the second trough of the "w" type oscillation at 8.2 ka BP. With the sharp decrease of the $\delta^{18}O$ value, the

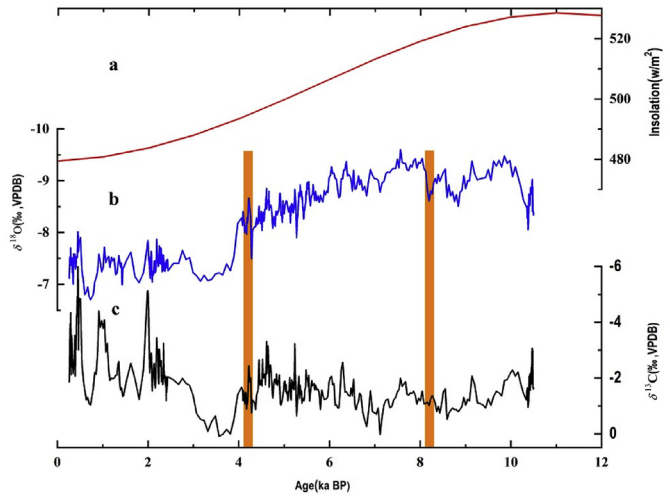

Fig. 3. Stalagmite J13 record vs. 21 July insolation at 65°N (red, W/m^2; Berger, 1978) over the last 11.0 ka BP. Shown are the stalagmite J13 $\delta^{18}O$ record (blue) and $\delta^{13}C$ record (black). Following the sub-division of the Holocene by Walker et al. (2019), 8.2 and 4.2 ka BP (orange bands) are taken as the respective boundaries of the early to middle Holocene and the middle to late Holocene. (For interpretation of the references to color in this figure legend, the reader is referred to the Web version of this article.)

"w" type oscillating change was abruptly terminated at approximately 8.2 ka BP. After this, $\delta^{18}O$ values decreased gradually and reached the second peak at 7.5 ka BP.

The lowest $\delta^{18}O$ values for the entire Holocene were observed during the period of 8.0–6.0 ka BP. Stalagmite J13 $\delta^{18}O$ values showed a gradual increase from 6.0 ka BP. Around 4.2 ka BP, $\delta^{18}O$ values increased sharply. The $\delta^{13}C$ of stalagmite J13 also showed a similar trend, which may be related to reduced karst activity and less soil-derived CO_2 caused by the weakening of monsoon. From c. 4.0 ka BP onwards, the stalagmite isotopic records show significant variability, though $\delta^{18}O$ values show an overall decreasing trend. During the entire Holocene, the $\delta^{13}C$ values range from 0.1‰ to −0.6‰, with the average being −1.8‰. There was a negative correlation between the $\delta^{13}C$ and $\delta^{18}O$ records of stalagmite J13 throughout the Holocene (Fig. s2). However, subsection correlation analysis shows that there is no correlation in the early-mid Holocene (Fig. s3), and shows a significant positive correlation in the late Holocene (Fig. s4). We speculate that monsoon precipitation may have a threshold effect on vegetation and soil biomass (Zhao et al., 2017). When monsoon precipitation is below a certain value, monsoon precipitation may become a key factor affecting vegetation and soil biomass, which needs further in-depth research to verify.

4. Discussion

4.1. Holocene monsoon weakening event

Although there is controversy about the interpretation of stalagmite $\delta^{18}O$ in the EASM region, there is a general consensus that stalagmite $\delta^{18}O$ values mainly reflect the intensity of the EASM (Cheng et al., 2009; Dykoski et al., 2005; Wang et al., 2001, 2005; Yang et al., 2019; Yuan et al., 2004). Chronostratigraphically, according to the International Stratigraphic Commission's division of the Holocene, 8.2 ka BP is regarded as the major division between the early and the mid-Holocene; whilst 4.2 ka BP is the major boundary between the mid and late Holocene (Walker et al., 2019) (Fig. 3).

The $\delta^{18}O$ record from stalagmite J13 shows a rapid transition to low values at the beginning of the Holocene (Fig. 3). However, the strengthening of the EASM reflected in the depleted $\delta^{18}O$ values was brief (~0.5 ka). The "w" type oscillation in the period of 9.1–8.1 ka BP implies a millennial-scale oscillation in the intensity of the EASM at the end of the early Holocene. This "w" type oscillation can be divided into two stages characterized by a weakening of the EASM (Figs. 3 and 4): 1) from 9.1-8.8 ka BP —the monsoon weakened for 0.3 ka before intensifying rapidly from 8.8-8.5 ka BP; and 2) at 8.5-8.2 ka BP, —the monsoon weakened for a similar duration. These two centennial-scale monsoon weakening events exhibit clear temporal symmetry. The early Holocene monsoon weakening events recorded by stalagmite J13 are significantly different to the 8.2 ka event reported previously (Cheng et al., 2009; Liu et al., 2013). For example, the "w" type oscillation began at 9.1 ka BP and lasted for nearly ~1.0 ka. In contrast, the 8.2 ka event lasted only 0.2 ka (Cheng et al., 2009; Liu et al., 2013). The oscillation noted at Jinfo Cave may also include the 8.2 ka event, implying that it was part of a longer phase of monsoon instability rather than a standalone abrupt change. The rapid shift to low $\delta^{18}O$ values thereafter until 6.0 ka BP implies a strengthening of the monsoon occurred abruptly in the mid-Holocene around the time of the "mid-Holocene optimum" (Chen et al., 2015; Shi et al., 1994). Thereafter, the stalagmite $\delta^{18}O$ values exhibit a gradual transition to high values, indicating a slow weakening of the monsoon. Overall, the stalagmite $\delta^{18}O$ record indicates that the monsoon was strongest during the early and mid-Holocene. Furthermore, the record suggests that the EASM was more stable in the mid-Holocene than in the early Holocene.

Moving to the mid-late Holocene period, the J13 $\delta^{18}O$ record shows significant shifts to higher values at 7.0 ka BP, 4.2 ka BP, 2.0 ka BP, and 0.6 ka BP, suggesting a series of weak monsoon events. Another "w" type monsoon oscillation apparently occurred near 7.0 ka BP, lasting

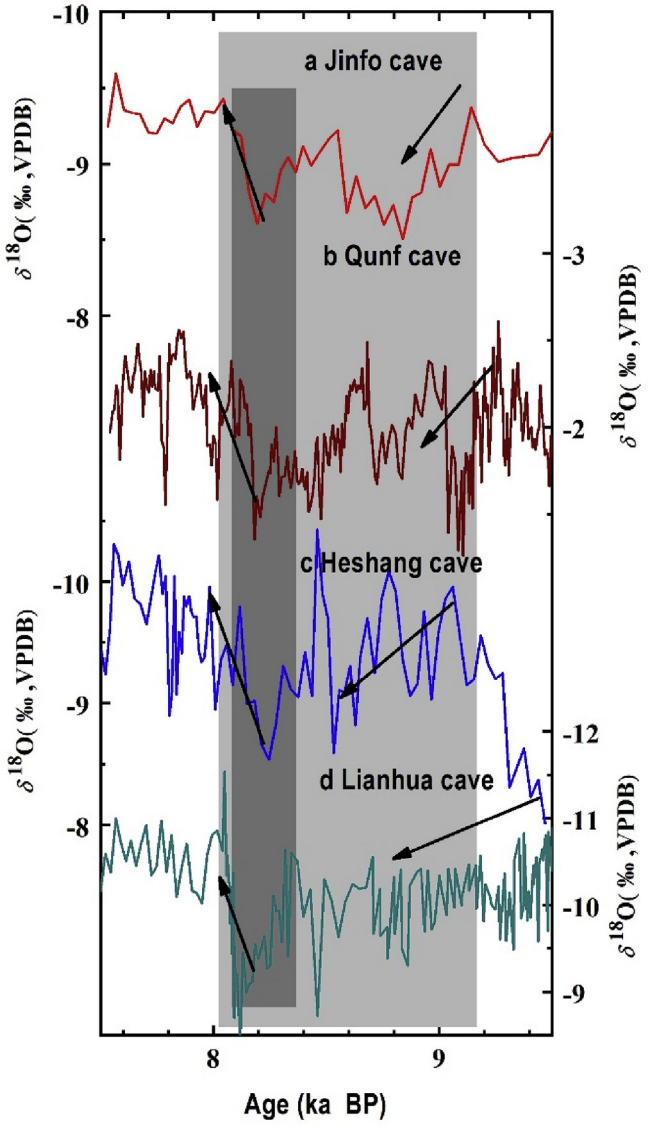

Fig. 4. Comparison of stalagmite records used to identify anomalies around 8.0–9.0 ka BP in Asian Monsoon Region. The light gray band indicates weak monsoon periods; dark gray band indicates the 8.2 ka event (Cheng et a1., 2009; Liu et a1., 2013). (a) Jinfo Cave (J13); (b) Qunf Cave (Q5) (Fleitmann et a1., 2003); (c) Heshang Cave (HS4) (Hu et a1., 2008); (d) Lianhua Cave (Dong et a1., 2015).

for about 0.5 ka. It is possible that this event may have acted as a key background for human adaptations in northern and southern China during the Neolithic period (Cheng et al., 2018; Dong et al., 2016, 2019). For example, Dong et al. (2016, 2019) have proposed that increased monsoonal activity and precipitation in northern China c. 7.0-6.0 ka BP promoted the expansion of rain-fed agriculture, and increasing land clearance. Similar behavioural changes have also been noted in the Zhujiang delta of southern China during the Neolithic period (Cheng et al., 2018). The 4.2 ka event apparent in the Jinfo record indicates a 1,000 year weakening of the monsoon, which may have played a role in the decline of the Neolithic in central China following this initial proliferation (Wang et al., 2001), although more detailed local paleoenvironmental studies would be required to test this proposition further.

There are apparently significant differences between the driving mechanisms of the 8.2 ka and 4.2 ka events noted in the Jinfo Cave record, and other Chinese records (Cheng et al., 2019a; Kathayat et al., 2018). The 8.2 ka event occurred in the early Holocene when the Laurentide ice sheet of the last glacial period had not yet completely melted and has been associated with the outbreak of freshwater (Alley et al., 1997; Cheng et al., 2009; Liu et al., 2013). Meanwhile, the 4.2 ka event occurred in the mid-Holocene, likely as a product of declining solar radiation and the movement of the inter-tropical convergence zone (ITCZ) southward (Cheng et al., 2019a; Kathayat et al., 2018). Nevertheless, both events are believed to also have been related to the weakening of the Atlantic Meridian Overturning Circulation (AMOC) (Barker, 2009; Stocker, 1998; Zarriess et al., 2011).

Stalagmite J13 $\delta^{18}O$ increases in the late Holocene, documenting significant fluctuations. A pronounced period of monsoon weakening occurred c. 0.6 ka BP, around the time of the 'Little Ice Age' (Zhang et al., 2008). Stalagmite J13 $\delta^{13}C$ is sensitive to events of weakening monsoon, showing increases during these periods. This is likely a product of reduced rainfall and temperature resulting in the reduced production of soil CO_2 (Raich and Schlesinger, 1992) and increased stalagmite $\delta^{13}C$ (Genty et al., 2003).

4.2. Comparison of the Holocene monsoon records in Asia

The changes in EASM registered in stalagmite J13 are also seen in other records from the EASM region. For instance, the stalagmite HS4 record with an average resolution of ~16 years (Fig. 5d) from the

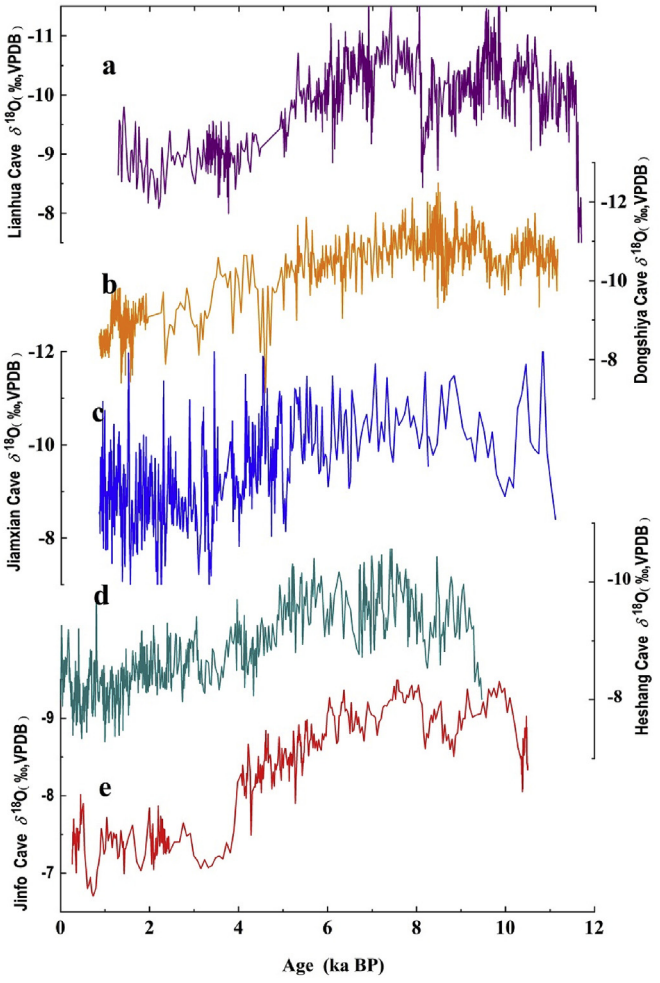

Fig. 5. Comparison of $\delta^{18}O$ records of stalagmites in the Chinese monsoon region. Shown are $\delta^{18}O$ records from (a) Lianhua Cave (38°10′N,113°43′E) (Dong et al., 2015); (b) Dongshiya Cave (33°47′N,111°34′E) (Zhang et al., 2018); (c) Jiuxian Cave (33°34′N,109°6′E) (Cai et al., 2010); (d) Heshang Cave (30°27′N,110°25′E) (HS4) (Hu et al., 2008); and (e) Jinfo Cave (29°01′N,107°11′E) (J13).

neighboring area shows a brief phase of intense EASM activity in the period of 9.1–8.7 ka BP during the early Holocene, followed by a distinct “w" type oscillation in the period of 8.7–8.1 ka BP (Hu et al., 2008). In addition, the stalagmite record from Jiuxian Cave in central China documents a short-term phase of intense EASM activity in the period of 11.0–10.2 ka BP followed by a “w" type oscillation in the period of 10.2–9.0 ka BP with an asymmetric “quick start and slow end” pattern (Fig. 5c) (Cai et al., 2010). Records from Lianhua Cave in northern China show two short periods of monsoon intensification in the early Holocene, at 9.8-9.4 and 10.7-10.2 ka BP, followed by a millennial-scale weakening monsoon phase with a “slow start and quick end” pattern which took place in the period of 9.5–8.1 ka BP (Fig. 5a) (Dong et al., 2018). The DSY2 and LM2 records (Fig. 5b) in Henan province also indicate two phases of enhanced EASM activity during the early Holocene in northern China (Zhang et al., 2018). When comparing records from northern and southern China, it is important to note that the influence of Indian Ocean water vapour, Pacific water vapour, and water vapour from westerlies, lead to more complicated interpretations of $\delta^{18}O$ for the former (Clemens et al., 2010). For instance, two phases of enhanced EASM activity are indicated in northern China. Moreover, the “w" type oscillations noted in the Jinfo Cave record are not as obvious (Dong et al., 2018; Zhang et al., 2018). In contrast, the single primary water vapour source of the Indian Ocean means that stalagmites from southern China, similar to those in Oman, are primarily indicative of strengthened monsoon activity in the early Holocene followed by a “w" type oscillation (Fleitmann et al., 2003; Hu et al., 2008).

Holocene Asian monsoon changes recorded by stalagmite J13 are also corroborated by lake (An et al., 2012; Chen et al., 2015; Hong et al., 2003) and ocean records (Gupta et al., 2003). For instance, the reconstructed EASM records from Gonghai Lake (Fig. 6a) document a short-term, moderate-intensity monsoon enhancement event occurred in the period of 10.2–9.5 ka BP, followed by a slight weakening in the period of 9.5–8.5 ka BP. Precipitation maxima occurred in the period of

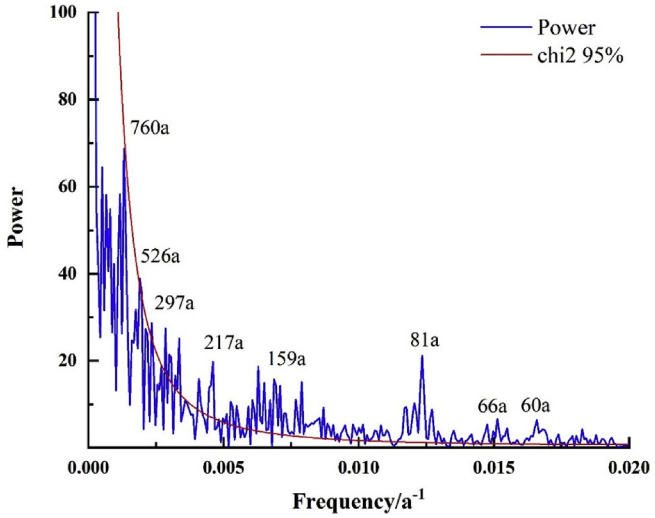

Fig. 7. Spectral analysis (Schulz and Mudelsee, 2002) (blue solid line) of the $\delta^{18}O$ records of stalagmite J13 from Jinfo Cave. (For interpretation of the references to color in this figure legend, the reader is referred to the Web version of this article.)

7.8–5.3 ka BP, indicating that the most intense monsoon conditions prevailed during the mid-Holocene (Chen et al., 2015). The Asian Summer Monsoon Index (SMI) reconstructed from Qinghai Lake (Fig. 6d) also shows that the intensity of the monsoon exhibited major fluctuations during the early Holocene, with alternating phases of weakening and strengthening (An et al., 2012). In summary, different geological archives from regions subjected to the Asian monsoon all reveal a similar spatio-temporal pattern of monsoon evolution comprising: (i) a brief phase of intense monsoon activity in the early Holocene; (ii) a weakening of the monsoon lasting for around 1.0 ka. Of

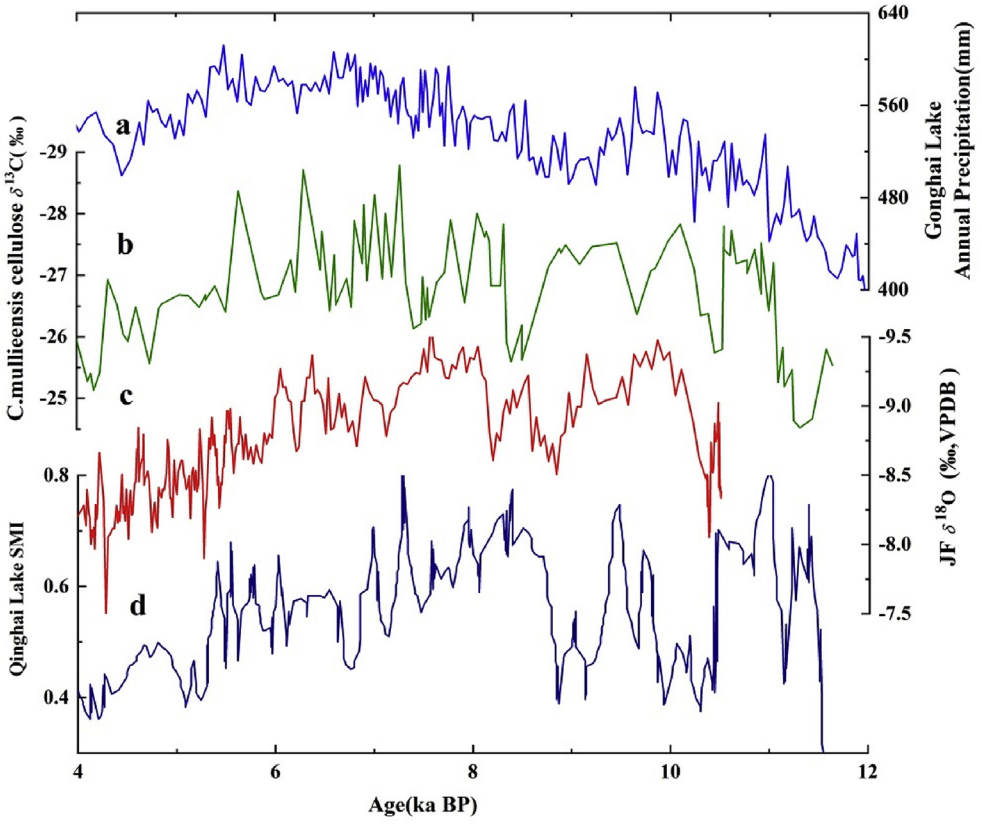

Fig. 6. Comparison of stalagmite J13 $\delta^{18}O$ with (a) quantitative precipitation reconstruction from Gonghai Lake, in North China (Chen et al., 2015); (b) $\delta^{13}C$ values of C.*mulieensis cellulose* from Hongyuan (Hong et al., 2003); (c) $\delta^{18}O$ records from Jinfo Cave; and (d) Asian Summer Monsoon Index (SMI) reconstructed from Qinghai Lake (An et al., 2012).

key importance is that the weakening of the monsoon during the early Holocene affected the entire EASM region.

4.3. Spectral analysis of stalagmite records

Spectral analysis results are shown in Fig. 7 (Hammer et al., 2001). Several cycles are evident (217a, 159a, 81a, 66a and 60a) over the last 10.5 ka,which exhibit significant periodicities (95% confidence level) and may be indicative of changes in solar activity (Agnihotri et al., 2002). Therefore, our data support the idea that solar changes are partly responsible for driving changes in the EASM during the Holocene. However, the existence of non-solar related periodicities (e.g. the 526a and 760a cycles) (Stuiver and Braziunas, 1993) also implies that the thermohaline circulation (THC) might also play a role in driving variations in EASM intensity. Many studies show that the Asian monsoon has a periodicity of c. 500 years (Dong et al., 2018; Fleitmann et al., 2003; Hu et al., 2008; Xu et al., 2019; Zhang et al., 2018). Research on the pollen record of Maar Lake and archaeological sites in Northeast China reveals that monsoonal cycling every 500 years may have had a regular impact on prehistoric human behaviour across the Holocene (Xu et al., 2019). Changes in the amount of freshwater input to the North Atlantic impacted changes in the EASM during the Holocene (Gupta et al., 2003; Hong et al., 2006; Wang et al., 2005, 2008). Increased freshwater input in the North Atlantic resulted in a weakening of the THC (Stocker, 1998). Due to the bipolar seesaw effect, warm ocean waters were blocked in the southern hemisphere and low-tropics. Eventually, the heat balance in the northern and southern hemispheres was broken, resulting in a southward shift of the ITCZ and a weakening of the EASM (Barker et al., 2009; Chao et al., 2000; Stocker, 1998; Zarriess et al., 2011). On the other hand, in the mid-high latitudes of the northern hemisphere, both the North Atlantic climate change and melt water from the ice sheets facilitated the strengthening of the Siberian high-pressure system. The strengthening of winter winds has also been shown to promote the southward shift of the ITCZ and accelerate the weakening of Asian monsoon intensity (Carlson et al., 2008; Chen et al., 2015; Denton et al., 2005; Dong et al., 2018).

5. Conclusion

We reconstructed the evolution of the EASM on the basis of a well-dated $\delta^{18}O$ record from stalagmite J13 in Jinfo Cave, southern China. Results were compared against other stalagmite, lake and peat records across the Asian monsoon region, from which the following conclusions are drawn:

1. The record of stalagmite J13 in southwestern China shows that the EASM exhibited a short intense phase in the period of 10.1–9.6 ka BP.
2. The EASM in the period of 9.1–8.1 ka BP exhibited a “w" type oscillation, indicating that the monsoon weakened. Based on this study and other monsoon records, it is proposed that the early Holocene monsoon weakening events are widespread in the EASM region.
3. The stalagmite record shows that the EASM intensified again in the period 8.0-6.0 ka BP. After 6.0 ka BP, the EASM gradually weakened, which suggests that there were strong widespread monsoon periods in the early and middle Holocene, respectively.

Declaration of competing interest

We declare that we do not have any commercial or associative interest that represents a conflict of interest in connection with the work submitted.

Acknowledgements

We thank two anonymous reviewers for their comments that helped improve the manuscript. This work was supported by National Key R&D Program of China (2016YFC0502301); grants from the National Natural Science Foundation of China (41971109, 41572158, 41272192 and 41072141). Holocene stalagmite $\delta^{18}O$ and the chronological data used to support the findings of this study can be obtained in the supporting information file (available online). All these data will be deposited in the World Data Center repository (https://www.ncdc.noaa.gov/data-access/paleoclimatology-data/datasets/speleothem).

Appendix A. Supplementary data

Supplementary data to this article can be found online at https://doi.org/10.1016/j.quaint.2020.01.002.

References

Agnihotri, R., Dutta, K., Bhushan, R., et al., 2002. Evidence for solar forcing on the Indian monsoon during the last millennium. Earth Planet. Sci. Lett. 198 (3), 521–527.
Alley, R.B., Mayewski, P.A., Sowers, T., 1997. Holocene Climatic Instability–a prominent, widespread event 8200 yr ago. Geology 25, 483–486 1997.
An, Z., Colman, S.M., Zhou, W., et al., 2012. Interplay between the westerlies and Asian monsoon recorded in lake Qinghai sediments since 32 ka. Sci. Rep. 2 (8), 619.
An, Z., Porter, S.C., Kutzbach, J.E., et al., 2000. Asynchronous Holocene optimum of the East asian monsoon. Quat. Sci. Rev. 19 (8), 743–762.
Barker, S., Diz, P., Vautravers, M., et al., 2009. Interhemispheric Atlantic seesaw response during the last deglaciation. Nature 457 (7233), 1097–1102.
Berger, A., 1978. Long-term variations of caloric insolation resulting from the Earth's orbital elements. Quat. Res. 9, 139–167.
Cai, Y., Tan, L.C., Cheng, H., et al., 2010. The variation of summer monsoon precipitation in central China since the last deglaciation. Earth Planet. Sci. Lett. 291 (1), 21–31.
Carlson, A.E., Oppo, D.W., Came, R.E., et al., 2008. Subtropical Atlantic salinity variability and Atlantic meridional circulation during the last deglaciation. Geology 36 (12), 991–994.
Chao, W.C., 2000. Multiple quasi equilibria of the ITCZ and the origin of monsoon onset. J. Atmos. Sci. 57 (5), 641–652.
Chen, C.J., Li, T.Y., 2018. Geochemical characteristics of cave drip water respond to ENSO based on a 6-year monitoring work in Yangkou Cave, Southwest China. J. Hydrol. 561, 896–907.
Chen, F.H., Xu, Q.H., Chen, J.H., et al., 2015. East Asian summer monsoon precipitation variability since the last deglaciation. Sci. Rep. 5, 11186.
Cheng, H., Edwards, R.L., Shen, C.C., et al., 2013. Improvements in ^{230}Th dating, ^{230}Th and ^{234}U half-life values, and U-Th isotopic measurements by multi-collector inductively coupled plasma mass spectroscopy. Earth Planet. Sci. Lett. 371, 82–91.
Cheng, H., Fleitmann, D., Edwards, R.L., et al., 2009. Timing and structure of the 8.2 kyr BP event inferred from $\delta^{18}O$ records of stalagmites from China, Oman, and Brazil. Geology 37 (11), 1007–1010.
Cheng, H., Sinha, A., Verheyden, S., et al., 2015. The climate variability in northern Levant over the past 20,000 years. Geophys. Res. Lett. 42, 8641–8650.
Cheng, H., Zhang, H., Zhao, J., et al., 2019a. Chinese stalagmite paleoclimate researches: a review and perspective. Sci. China Earth Sci. 1–25.
Cheng, H., Springer, G., Sinha, A., et al., 2019b. Eastern North American climate in phase with fall insolation throughout the last three glacial-interglacial cycles. Earth Planet. Sci. Lett. 522, 125–134.
Cheng, Z.J., Weng, C.Y., Steinke, S., et al., 2018. Anthropogenic modification of vegetated landscapes in southern China from 6,000 years ago. Nat. Geosci. 11 (12), 939–943.
Clemens, S.C., Prell, W.L., Sun, Y., 2010. Orbital-scale timing and mechanisms driving Late Pleistocene Indo-Asian summer monsoons: reinterpreting cave speleothem $\delta^{18}O$. Paleoceanography 25, PA4207. https://doi.org/10.1029/2010PA001926.
Denton, M.H., Thomsen, M.F., Korth, H., et al., 2005. Bulk plasma properties at geosynchronous orbit. Geophysical Research 110, A07223.
Dong, G.H., Li, R., Lu, M.X., et al., 2019. Evolution of human–environmental interactions in China from the late paleolithic to the bronze age. Prog. Phys. Geogr. 1–18. https://doi.org/10.1177/0309133319876802.
Dong, G.H., Zhang, S.J., Yang, Y.S., et al., 2016. Agricultural intensification and its impact on environment during Neolithic Age in northern China. Chin. Sci. Bull. 61, 2913–2925.
Dong, J.G., Shen, C.C., Kong, X.G., et al., 2015. Reconciliation of hydroclimate sequences from the Chinese loess plateau and low-latitude East Asian summer monsoon regions over the past 14,500 years. Palaeogeogr. Palaeoclimatol. Palaeoecol. 435 (3), 127–135.
Dong, J.G., Shen, C.C., Kong, X.G., et al., 2018. Rapid retreat of the East Asian summer monsoon in the middle Holocene and a millennial weak monsoon interval at 9 ka in northern China. J. Asian Earth Sci. 151, 31–39.
Dreybrodt, W., 1982. A possible mechanism for growth of calcite speleothems without participation of biogenic carbon dioxide. Earth Planet. Sci. Lett. 58, 293–299.
Dykoski, C.A., Edwards, R.L., Cheng, H., et al., 2005. A high-resolution, absolute-dated Holocene and deglacial Asian monsoon record from Dongge Cave, China. Earth

Planet. Sci. Lett. 233 (1), 71–86.
Fleitmann, D., Burns, S.J., Mudelsee, M., et al., 2003. Holocene forcing of the Indian monsoon recorded in a stalagmite from southern Oman. Science 300 (5626), 1737–1739.
Genty, D., Blamart, D., Ouahdi, R., 2003. Precise dating of Dansgaard-Oeschger climate oscillations in the western Europe from stalagmite data. Nature 421, 833–837.
Goldsmith, Y., Broecker, W.S., Xu, H., et al., 2017. Northward extent of East Asian monsoon covaries with intensity on orbital and millennial timescales. Proc. Natl. Acad. Sci. 114 (8), 1817–1821.
Gupta, A.K., Anderson, D.M., Overpeck, J.T., 2003. Abrupt changes in the asian southwest monsoon during the Holocene and their links to the north atlantic ocean. Nature 421 (6921), 354–357.
Hammer, ϕ, Harper, D.A., Ryan, P.D., 2001. PAST: palaeontological Statistics software package for education and data analysis. Palaeontol. Electron. 4 (1), 1–9.
Hendy, C.H., 1971. The isotopic geochemistry of speleothems-I. The calculation of the effects of different modes of formation on the isotopic composition of speleothems and their applicability as palaeoclimatic indicators. Geochem. Cosmochim. Acta 35 (8), 801–824.
Hercman, H., Pawlak, J., 2012. MOD-AGE: an age-depth model construction algorithm. Quat. Geochronol. 12, 1–10.
Hong, Y.T., Hong, B., Lin, Q.H., et al., 2003. Correlation between Indian ocean summer monsoon and North Atlantic climate during the Holocene. Earth Planet. Sci. Lett. 211 (3–4), 371–380.
Hong, Y.T., Hong, B., Lin, Q.H., 2006. Inverse phase oscillations between the East Asian and Indian Ocean summer monsoons during the last 12000 years and paleo-El Nino. Earth Planet. Sci. Lett. 231, 337–346.
Hu, C.Y., Henderson, G.M., Huang, J., et al., 2008. Quantification of Holocene Asian monsoon rainfall from spatially separated cave records. Earth Planet. Sci. Lett. 266 (3), 221–232.
Kathayat, G., Cheng, H., Sinha, A., et al., 2018. Evaluating the timing and structure of the 4.2 ka event in the Indian summer monsoon domain from an annually resolved speleothem record from Northeast India. Clim. Past 14 (12), 1869–1879.
Li, T.Y., Li, H., Xiang, X., et al., 2012. Transportation characteristics of $\delta^{13}C$ in the plants-soil-bedrock-cave system in Chongqing karst area. Sci. China Earth Sci. 2012 (55), 685–694.
Liu, Y.H., Henderson, G.M., Hu, C.Y., et al., 2013. Links between the East asian monsoon and North Atlantic climate during the 8,200-year event. Nat. Geosci. 6 (2), 117–120.
Lu, H.Y., Yi, S.W., Liu, Z.Y., et al., 2013. Variation of East Asian monsoon precipitation during the past 21 k.y. and potential CO_2 forcing. Geology 41 (9), 1023–1026.
Maher, B.A., 2008. Holocene variability of the East Asian summer monsoon from Chinese cave records: a re-assessment. Holocene 18 (6), 861–866. https://doi.org/10.1177/0959683608095569.
Maher, B.A., Thompson, R., 2012. Oxygen isotopes from Chinese caves: records not of monsoon rainfall but of circulation regime. J. Quat. Sci. 27, 615–624.
Perez-Mejías, C., Moreno, A., Sancho, C., et al., 2018. Transference of isotopic signal from rainfall to dripwaters and farmed calcite in Mediterranean semi-arid karst. Geochem. Cosmochim. Acta 243, 66–98.
Raich, J., Schlesinger, W., 1992. The global carbon dioxide flux in soil respiration and its relationship with vegetation and climate. Tellus 44B, 81–99.
Schulz, M., Mudelsee, M., 2002. REDFIT: estimating red-noise spectra directly from unevenly spaced paleoclimatic time series. Comput. Geosci. 28, 421–426.
Shen, C.C., Wu, C.C., Cheng, H., et al., 2012. High-precision and high resolution carbonate ^{230}Th dating by MC-ICP-MS with SEM protocols. Geochem. Cosmochim. Acta 99, 71–86.
Shi, Y.F., Kong, Z.C., Wang, S.M., et al., 1994. Climates and environments of the Holocene mega thermal maximum in China. Sci. China Chem. 37 (4), 481–493.
Stocker, T.F., 1998. Climate change: the seesaw effect. Science 282 (5386), 61–62. https://doi.org/10.1126/science.282.5386.61.
Stuiver, M., Braziunas, T.F., 1993. Sun, ocean, climate and atmospheric CO_2: anevaluation of causal and spectral relationships. *Holocene* 3 (4), 289–305.
Tan, M., 2009. Circulation effect: climatic significance of the short term variability of the oxygen isotopes in stalagmites from monsoonal China. J. Quat. Sci. 29 (5), 851–862.
Walker, M., Gibbard, P., Head, M.J., et al., 2019. Formal subdivision of the Holocene series/epoch: a summary. J. Geol. Soc. India 93 (2), 135–141.
Wang, Y.J., Cheng, H., Edwards, R.L., et al., 2001. A high-resolution absolute-dated late Pleistocene Monsoon record from Hulu Cave, China. Science 294 (5550), 2345.
Wang, Y.J., Cheng, H., Edwards, R.L., et al., 2005. The Holocene Asian monsoon: links to solar changes and North Atlantic climate. Science 308 (5723), 854.
Wang, Y.J., Cheng, H., Edwards, R.L., et al., 2008. Millennial-and orbital-scale changes in the East Asian monsoon over the past 224,000 years. Nature 451 (7182), 1090.
Xu, D.K., Lu, H.Y., Chu, G.Q., et al., 2019. Synchronous 500-year oscillations of monsoon climate and human activity in Northeast Asia. Nat. Commun. 10, 4105.
Yang, X.L., Liu, J.B., Liang, F.Y., et al., 2014. Holocene stalagmite $\delta^{18}O$ records in the East Asian monsoon region and their correlation with those in the Indian monsoon region. Holocene 24 (12), 1657–1664. https://doi.org/10.1177/0959683614551222.
Yang, X.L., Yang, H., Wang, B.Y., et al., 2019. Early-Holocene monsoon instability and climatic optimum recorded by Chinese stalagmites. Holocene 29 (6), 1059–1067.
Yuan, D.X., Cheng, H., Edwards, R.L., et al., 2004. Timing, duration, and transitions of the last interglacial Asian monsoon. Science 304 (23), 575–578.
Zanchetta, G., Drysdale, R.N., Hellstrom, J.C., et al., 2007. Enhanced rainfall in the Western Mediterranean during deposition of sapropel S1: stalagmite evidence from Corchia cave (Central Italy). Quat. Sci. Rev. 26 (3–4), 280–286.
Zarriess, M., Johnstone, H., Prange, M., et al., 2011. Bipolar seesaw in the northeastern tropical Atlantic during Heinrich stadials. Geophys. Res. Lett. 38, L04706. https://doi.org/10.1029/2010GL046070.
Zhang, J., Chen, F., Holmes, J., et al., 2012. Holocene monsoon climate documented by oxygen and carbon isotopes from lake sediments and peat bogs in China: a review and synthesis. Quat. Sci. Rev. 30 (15–16), 1973–1987.
Zhang, N., Yang, Y., Cheng, H., et al., 2018. Timing and duration of the East Asian summer monsoon maximum during the Holocene based on stalagmite data from North China. Holocene 28 (10), 1631–1641.
Zhang, P.Z., Cheng, H., Edwards, R.L., et al., 2008. A test of climate, sun, and culture relationships from an 1810-year Chinese cave record. Science 322, 940–942.
Zhang, Y.H., Yang, Y., Yang, X.L., et al., 2015. Early Holocene monsoon evolution of high-resolution stalagmite $\delta^{18}O$ records: in henan Laomu cave. Acta Sedimentol. Sin. 33 (1), 134–141.
Zhao, Y., Liu, Y., Guo, Z., et al., 2017. Abrupt vegetation shifts caused by gradual climate changes in central Asia during the Holocene. Sci. China Earth Sci. 60 (7), 1317–1327. https://doi.org/10.1007/s11430-017-9047-7.
Zhou, W., Yu, X., Jull, A.T., et al., 2004. High-resolution evidence from southern China of an early Holocene optimum and a mid-Holocene dry event during the past 18,000 years. Quat. Res. 62 (1), 39–48.